

Laminar Flow with Injection Through A Long Dead-End Cylindrical Porous Tube: Application to a Hollow Fiber Membrane

Albert S. Kim

Dept. of Civil and Environmental Engineering, College of Engineering,
University of Hawaii at Manoa, Honolulu, HI 96822, and

Dept. of Chemical Engineering, College of Engineering, Kyung Hee University, Gyeonggi-do 449-701, Korea

Yong Taek Lee

Dept. of Chemical Engineering, College of Engineering, Kyung Hee University, Gyeonggi-do 449-701, Korea

DOI 10.1002/aic.12430

Published online November 2, 2010 in Wiley Online Library (wileyonlinelibrary.com).

Effects of membrane length and hydraulic resistance on the steady-state laminar flow of a fluid with injection in a dead-end cylindrical porous tube have been investigated using the perturbation approach of the Navier-Stokes and continuity equations. Analytic solutions of the dynamic equations, reduced to non linear differential equations, were obtained and applied to submerged, dead-end hollow fiber membranes of large resistances and small wall Reynolds numbers. The velocity and pressure profiles were solved using the method of separation of variables as with physical properties of the membrane and fluid and the wall velocity at the dead end. The constant flux approximation was found to be valid only for a short membrane with a large hydraulic resistance. The constant permeability approximation used in this study is universal for a membrane of an arbitrary length, through which the fluid velocities and pressure increase exponentially from the dead end to the open end. © 2010 American Institute of Chemical Engineers AICHE J, 57: 1997–2006, 2011

Keywords: hollow fiber membrane, laminar flow, injection, Navier-Stokes equation, perturbation

Introduction

Among various configurations of membrane modules, hollow fiber (HF) membranes are used for applications in a variety of fields, including membrane distillation,^{1,2} wine filtration,³ juice upgrading,⁴ pharmaceutical processing,^{5–7} and water and wastewater treatment.^{8–12} Recently, forward osmosis processes received close attention because of low-pressure requirement and cost effectiveness,^{13,14} and module de-

velopment of forward osmosis HF membranes are currently in an active stage.^{15–17} Advantages of using HF membranes include extremely large packing densities and simple operational methods. Especially, in water and wastewater treatment, a bundle of dead-end HF membranes is submerged in a tank, and a negative pressure is applied to each fiber's interior to generate a pressure gradient. A permeate flow entering from the exterior to the interior of the HF membrane wall produces an internal crossflow, and the crossflow rate substantially increases from the fiber's dead end to the open end. The permeate flux (i.e., wall velocity) from the porous wall dominates the crossflow velocity near the dead end, but becomes negligible in comparison with the crossflow velocity toward

Correspondence concerning this article should be addressed to Y. T. Lee at yongtlee@khu.ac.kr.

Table 1. A Comparison of this Study with Previous Work

	Berman (Ref. 23)	Yuan and Finkelstein (Ref. 24)	Karode (Ref. 52)	This Study
Geometry	Rectangular slit of semi-infinite width with two equally porous walls	Porous cylindrical tube	Porous rectangular slit and cylindrical tube	Cylindrical tube of a uniform permeability as applied to a hollow fiber membrane module
Governing equations	Navier-Stokes and continuity equations, Eqs. 1–3	Navier-Stokes and continuity equations, Eqs. 1 and 2	Fluid mass balance equation	Navier-Stokes and continuity equations, Eqs. 3–5
Wall Reynolds number regions	small ($R_w \ll 1$)	small ($R_w \ll 1$) and large ($R_w \gg 1$)	Not specified	small ($R_w \ll 1$)
Flow type	2D, incompressible, steady-state, laminar flow	2D, incompressible, steady-state, laminar flow	2D, incompressible, steady-state, laminar flow	2D, incompressible, steady-state, laminar flow
Assumption	Constant wall velocity	Constant wall velocity	Constant wall permeability	Constant wall permeability
Perturbation function, f	Equation 30	Equations 25 and 38 for small and large R_w , respectively (same hereafter)	N/A	Equation 34
Cross-flow velocity	Equation 32	Equations 27 and 40	N/A	Equation 37
Permeate velocity	Equation 33	Equations 28 and 41	N/A	Equation 38
Pressure	Equation 37	Equations 30 and 41	Equations 10 and 14 for the slit and tube, respectively.	Equation 39

Equation numbers are associated with the particular references.

the open end. Analytic research on the fluid velocities and pressures in a long, dead-end HF membrane is of crucial necessity to obtain a deeper understanding of the internal crossflow and fouling phenomena.^{18–22} However, to date, only a limited amount of theoretical research on the effects of membrane length and resistance on crossflow rate and pressure distribution has been carried out. A brief literature review follows.

In 1953, Berman²³ investigated laminar flow in a rectangular channel with two uniformly porous walls of equal permeability. His work focused on cases of small wall Reynolds numbers due to a slow wall velocity regarded as a perturbation to the fast crossflow. Berman's primary assumptions included: (1) a steady-state flow, (2) an incompressible fluid, (3) the absence of external forces exerted on the fluid, (4) a laminar flow, and (5) a constant wall "velocity" (called in this study constant flux approximation (CFA)). Although Berman's work was limited to the fluid flow leaving the wall (i.e., inside-out permeation), Yuan and Finkelstein (YF)²⁴ used a similar perturbation technique with cylindrical coordinates and investigated suction (inside-out) as well as injection (outside-in) flow of low- and high-wall Reynolds numbers. Later, Berman²⁵ commented that "Good agreement is obtained between Yuan's predictions and the results of (Berman's) numerical integrations for large injection but not for large suction Reynolds numbers." Terrill and Thomas²⁶ transformed the two-point boundary value problem into an initial value problem, provided fundamentally more rigorous analysis (than Berman's²⁵) of numerical and theoretical solutions of YF's problem²⁴ with an arbitrary wall Reynolds number, and showed the existence of multiple numerical solutions based on the initial guesses using the no-slip boundary condition at the porous wall. Recent theoretical achievements on the fluid flow in permeable tubes include Chellam and Liu's work regarding slip effects on existence and multiplicity of the similarity solutions,²⁷ which concluded that the slip boundary condition on the permeable wall only weakly influences the transition wall Reynolds number of the flow re-

versal²⁸ with minimal changes in the similarity solutions. In parallel with the further theoretical development from YF's original work on laminar flow through porous wall, noticeable applications of YF's research include a plethora of engineering processes: crossflow ultrafiltration of particulate materials^{29–32}; computational fluid mechanics modeling in membrane channels and module design^{33–35}; fouling behavior of reverse osmosis membranes³⁶; constant properties of duct flow,³⁷ and laminar elasticoviscous,³⁸ pulsatile,³⁹ compressible,⁴⁰ and oscillatory⁴¹ flows in permeable channels; laminar heat transfer,^{42,43} combustion,⁴⁴ and gas/vapor separation⁴⁵; food science⁴⁶; and medical applications such as the uptake of tritium-cholesterol on the arterial wall,⁴⁷ convective flow and solute concentration in the (bioartificial) kidney,^{48–50} and the role of the "resting" eccrine sweat gland in thermoregulation.⁵¹

Although studies on the laminar flow through porous channels have been limited to CFA, Karode⁵² relaxed Berman's fifth assumption (i.e., constant flux) and used the constant permeability approximation (CPA). This was because the wall velocity is proportional to the trans-membrane pressure profile and increases dramatically along the axial direction.⁵³ Because Karode's analysis was based on fluid mass balance, as extended from the Hagen-Poiseuille equation, only mean fluid velocities were investigated without detailed analysis of the internal flow. Aforementioned theoretical studies (in comparison with this work) on quiescent fluid flows through porous ducts are summarized in Table 1 for various factors.

Although the excellent theoretical work of Berman,²⁵ YF,²⁴ and Karode⁵² provided fundamentals as well as practical aspects of the laminar flow through porous channels, to the best of our knowledge validity of their approaches in terms of the membrane length and resistance was not yet studied systematically. Focusing on the long dead-end HF membrane module of a constant permeability, therefore, we have in this study used YF's perturbation technique using cylindrical coordinates, provided analytic expressions of the pressure and velocity components for small wall Reynolds

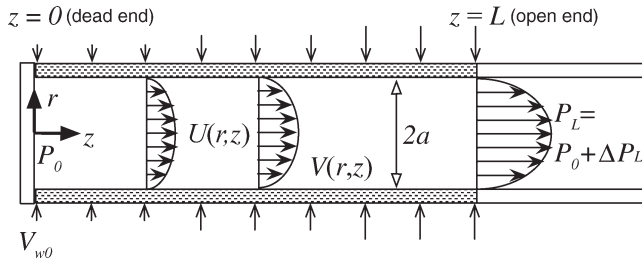


Figure 1. A schematic of injection flow (outside-in) of fluid with density ρ and dynamic viscosity ν through a long, dead-end porous cylindrical tube (i.e., hollow fiber membrane) of length L and resistance R_m .

U and V are fluid velocities in the axial and radial directions, respectively, and P is the pressure.

numbers, and discussed practical implications of the results from CPA.

Theory

Equations of motion

Figure 1 shows a schematic injection flow through a uniformly porous cylindrical tube with the entrance blocked, analogous to a submerged, long dead-end HF membrane. Negative pressure is applied to the interior at the open end ($z = L$), and it generates a permeate flux that increases from the dead end ($z = 0$). The crossflow velocity at the open end is equal to the integration of the permeate flux over the entire cylindrical porous wall, divided by the channel cross-sectional area.

For the sake of mathematical simplicity, we used the following dimensionless coordinate variables

$$\xi = \frac{z}{a} \quad (1)$$

$$\eta = \frac{r^2}{a^2} \quad (2)$$

where z and r are axial and radial coordinates, and a is the tube radius. We then rewrote the continuity and Navier-Stokes equations in cylindrical coordinates with axisymmetry for two-dimensional steady flow of a viscous incompressible fluid:

$$2\sqrt{\eta} \frac{\partial v}{\partial \eta} + \frac{v}{\sqrt{\eta}} + \frac{\partial u}{\partial \xi} = 0 \quad (3)$$

and

$$-\frac{\partial p}{\partial \xi} = u \frac{\partial u}{\partial \xi} + 2\sqrt{\eta} v \frac{\partial u}{\partial \eta} - \frac{1}{R_w} \left[4 \frac{\partial}{\partial \eta} \left(\eta \frac{\partial u}{\partial \eta} \right) + \frac{\partial^2 u}{\partial \xi^2} \right] \quad (4)$$

$$-\frac{\partial p}{\partial \eta} = u \frac{\partial}{\partial \xi} \left(\frac{v}{2\sqrt{\eta}} \right) + v \frac{\partial v}{\partial \eta} - \frac{1}{R_w} \left[2 \frac{\partial^2}{\partial \eta^2} (\sqrt{\eta} v) + \frac{\partial^2}{\partial \xi^2} \left(\frac{v}{2\sqrt{\eta}} \right) \right] \quad (5)$$

respectively, where $u(= U/V_{w0})$ and $v(= V/V_{w0})$ are dimensionless fluid velocities scaled by the permeate flux at the dead

end V_{w0} , $R_w(= aV_{w0}/\nu)$ is the wall Reynolds number, and $p(= P/\rho V_{w0}^2)$ is the dimensionless pressure (See Appendix A for the transformation of the Navier-Stokes and continuity equations between (r, z) and (η, ξ) coordinate systems.). Boundary conditions employed for u and v are:

$$u(\eta = 1) = 0 \quad (6)$$

$$v(\eta = 1, \xi = 0) = -1 \quad (7)$$

$$v(\eta = 0) = 0 \quad (8)$$

$$\sqrt{\eta} \frac{\partial u}{\partial \eta} \Big|_{\eta=0} = 0 \quad (9)$$

which imply that, on the membrane surface ($\eta = 1$), the axial velocity vanishes due to the no-slip boundary condition and the permeate flux at the dead end is a non-zero constant, i.e., V_{w0} ; and that, at the channel epi-center ($\eta = 0$), the radial velocity vanishes due to symmetry and the axial velocity reaches its maximum. The negative sign of Eq. 7 indicates the radial direction from the membrane wall to the epi-center. Analytic derivation of axisymmetric solutions for u , v , and p using the aforementioned boundary conditions is the primary objective of this study.

Once u and v are calculated using the boundary conditions, the cross-section averaged axial velocity \bar{u} and the length-averaged radial velocity \bar{v} can be calculated in dimensionless forms according to

$$\bar{u} = \int_0^1 u(\eta, \xi) d\eta \quad (10)$$

$$\bar{v} = \frac{1}{\xi} \int_0^\xi v(\eta = 1, \xi') d\xi' \quad (11)$$

where the prime indicates a dummy variable for integration.

Flow field in a dead-end hollow fiber module

For the dead-end HF membrane module as shown in Figure 1, one may represent the magnitude of the dimensionless wall velocity as

$$v_w(\xi) = -\frac{V}{V_{w0}} = \cosh \beta \xi \quad (12)$$

where β is a dimensionless transport parameter defined as⁵⁴

$$\beta = \frac{4}{\sqrt{R_m a}} \quad (13)$$

where R_m is the membrane resistance in a unit of inverse length (See Appendix B for detailed derivation of Eq. 12). Then, the dimensionless crossflow rate is calculated as

$$q(\xi) = \frac{Q}{\pi a^2 V_{w0}} = 2 \int_0^\xi v_w(\xi') d\xi' = \left(\frac{2}{\beta} \right) \sinh \beta \xi \quad (14)$$

which is the crossflow rate, Q , divided by the channel cross-sectional area, πa^2 , multiplied with the characteristic permeate velocity, V_{w0} .

At this point, the Stokes stream function for a two-dimensional axisymmetric flow may be introduced:

$$vV_{w0} = -\frac{1}{r} \frac{\partial \psi}{\partial z} = -\frac{1}{a^2 \sqrt{\eta}} \frac{\partial \psi}{\partial \xi} \quad (15)$$

$$uV_{w0} = +\frac{1}{r} \frac{\partial \psi}{\partial r} = +\frac{2}{a^2} \frac{\partial \psi}{\partial \eta} \quad (16)$$

which satisfy the continuity Eq. 3. Using the method of separation of variables, we propose a stream function:

$$\psi = \frac{1}{\pi} Q(\xi) f(\eta) = \left(\frac{2a^2 V_{w0}}{\beta} \right) f(\eta) \sinh \beta \xi \quad (17)$$

and its dimensionless form:

$$\Psi = \frac{\psi}{2a^2 \beta^{-1} V_{w0}} = f(\eta) \sinh \beta \xi \quad (18)$$

where $f(\eta)$ is the perturbation function.^{23,24} Then, u and v are represented using Ψ as:

$$u = \frac{4}{\beta} \frac{\partial \Psi}{\partial \eta} = 4f' \frac{\sinh \beta \xi}{\beta} \quad (19)$$

$$v = -\frac{2}{\beta} \frac{1}{\sqrt{\eta}} \frac{\partial \Psi}{\partial \xi} = -2 \frac{f}{\sqrt{\eta}} \cosh \beta \xi \quad (20)$$

The perturbation function f should satisfy the following boundary conditions, physically identical to Eqs. 6–9:

$$f'(1) = 0 \quad (21)$$

$$f(1) = \frac{1}{2} \quad (22)$$

$$\lim_{\eta \rightarrow 0} \frac{f(\eta)}{\sqrt{\eta}} = 0 \quad (23)$$

$$\lim_{\eta \rightarrow 0} \sqrt{\eta} f''(\eta) = 0 \quad (24)$$

respectively. By integrating u and v with respect to η and ξ , respectively, the averaged velocity components are calculated from Eqs. 10 and 11:

$$\bar{u} = 2 \frac{\sinh \beta \xi}{\beta} \quad (25)$$

$$\bar{v} = -\frac{\sinh \beta \xi}{\beta \xi} = -\frac{\bar{u}}{2\xi} \quad (26)$$

at the dimensionless distance ξ from the dead end. Multiplying $\pi a^2 V_{w0}$ with \bar{u} of Eq. 25 provides the crossflow rate Q at an arbitrary ξ , and the negative sign of Eq. 26 indicates the outside-in direction of the permeate flux. The (positive) ratio of \bar{u} to $-\bar{v}$ linearly increases from the dead end to the open end:

$$-\frac{\bar{u}}{\bar{v}} = 2\xi \quad (27)$$

which is one at the distance equal to the tube half-radius ($\xi = 1/2$), and is much larger than one near the open end ($\xi \gg 1$).

Table 2. Orders of Magnitude Analysis for Filtration Parameters of HF Membranes

	MF/UF	NF/RO
$R_m(\text{m}^{-1})$	10^{11} – 10^{12}	10^{13} – 10^{14}
$a(\text{m})$	10^{-4}	10^{-4}
$l(\text{—})$	10^3 – 10^4	10^3 – 10^4
$J_0(\mu\text{m}/\text{sec})$	10^1 – 10^2	10^0 – 10^1
$R_w(=J_0 a/v)(\text{—})$	10^{-3} – 10^{-2}	10^{-4} – 10^{-3}
$\lambda(\text{m}^{-1})$	10^0 – 10^1	10^{-1} – 10^0
$\beta(\text{—})$	10^{-4} – 10^{-3}	10^{-5} – 10^{-4}
$\beta l(\text{—})$	$\sim 10^0$	$\sim 10^{-1}$

$J_0(= \Delta P/\mu R_m)$ represents a typical value for the length-averaged permeate flux of pure solvent, where ΔP is the transmembrane pressure. Membrane resistance values are estimated using membrane permeability and flux data (especially, 80–170 L/m² h for UF³⁵) included in Refs. 55–57; the order of radius magnitude was taken from the classification of HF membrane ($a < 0.25$ mm)⁵⁸; and the membrane length is set to 1.0 m to estimate l .

By substituting u and v of Eqs. 19 and 20 into the Navier-Stokes Eqs. 4 and 5, we calculated the pressure gradients:

$$\frac{\partial p}{\partial \xi} = -16 \frac{\sinh \beta \xi}{\beta} \left[\cosh \beta \xi (f'^2 - ff'') - \frac{1}{R_w} \left(\eta f'''' + f'' + \frac{\beta^2}{4} f' \right) \right] \quad (28)$$

$$\frac{\partial p}{\partial \eta} = 4 \left[\frac{f^2}{2\eta^2} \cosh^2 \beta \xi - \frac{ff'}{\eta} - \frac{\cosh \beta \xi}{R_w} \left(f'' + \frac{\beta^2 f}{4\eta} \right) \right] \quad (29)$$

If the membrane length is short enough to satisfy $\beta l \ll 1$ where $l(= L/a)$ is the dimensionless length, i.e., the membrane length scaled by the tube radius, the pressure, and axial velocity linearly increase along the axial direction with the permeate flux of a pseudo constant.^{23,24}

Perturbation approach for a small Reynolds number, R_w

Partial differentials of Eqs. 28 and 29 with respect to η and ξ , respectively, are equal to each other, i.e., $\frac{\partial^2 p}{\partial \eta \partial \xi} = \frac{\partial^2 p}{\partial \xi \partial \eta}$, because the pressure is presumed to be a continuous function within the HF membrane channel. This equality yields:

$$\eta f'''' + 2f'''' + \frac{\beta^2}{2} f'' + \frac{\beta^4 f}{16\eta} = R_w \cosh \beta \xi \left[f' f'' - ff'''' + \frac{\beta^2 f^2}{4\eta^2} \right] \quad (30)$$

in which magnitudes of β , βl , and R_w are important semi-independent parameters that need further analytic development. In general, strict application of the separation of variables fails because both variables are present in Eq. 30. Nevertheless, the following practical features allow us to attempt reasonable approximations.

Table 2 shows the orders of magnitude of the characteristic parameters for the pressure-driven membrane filtration processes: microfiltration (MF), ultrafiltration (UF), nanofiltration (NF), and reverse osmosis (RO). Although the MF/UF group usually has membrane resistance one order of magnitude smaller than that of the NF/RO group, both membrane groups have intrinsic resistances large enough to satisfy the following two perturbation conditions:

- (i) $R_w \cosh \beta \xi \leq R_w \cosh \beta l \sim R_w O(1) \ll 1$, and
- (ii) $\beta^4 \ll \beta^2$ (equivalently $\beta^2 \ll 1$).

Condition (i) nullifies the right-hand-side of Eq. 30 to render:

$$\eta f'''' + 2f''' + \frac{\beta^2}{2}f'' + \frac{\beta^4}{16\eta}f = 0 \quad (31)$$

A general solution for f satisfying the full perturbation equation (Eq. 31) is calculated using Maple software version 13 (Maplesoft, Waterloo, Canada) as

$$\begin{aligned} f(\eta) = & B_1\sqrt{\eta}J_1(\beta\sqrt{\eta}) + B_2\sqrt{\eta}Y_1(\beta\sqrt{\eta}) \\ & + \left[B_3\left(-J_1(\beta\sqrt{\eta})\eta + \eta^{3/2}J_0(\beta\sqrt{\eta})\beta\right) \right. \\ & \left. + B_4\left(-Y_1(\beta\sqrt{\eta})\eta + \eta^{3/2}Y_0(\beta\sqrt{\eta})\beta\right) \right] \\ & \times \left[Y_1(\beta\sqrt{\eta})J_0(\beta\sqrt{\eta}) - J_1(\beta\sqrt{\eta})Y_0(\beta\sqrt{\eta}) \right] \quad (32) \end{aligned}$$

for which unknown constants, B_1 – B_4 , can be calculated by applying the same boundary conditions of Eqs. 21–24, but are left undetermined in this study. Instead, we take an advantage of condition (ii) to further neglect the fourth term of β^4 in Eq. 31 for a simpler mathematical process. Considering only the zeroth- and second-order terms of β in Eq. 31, one can calculate the general solution for

$$f(\eta) = C_1 + C_2\eta + C_3\sqrt{\eta}J_1(\alpha\sqrt{\eta}) + C_4\sqrt{\eta}Y_1(\alpha\sqrt{\eta}) \quad (33)$$

where J_1 and Y_1 are the first and second kinds of the first-order Bessel functions, respectively, and $\alpha = \beta\sqrt{2}$. This simpler solution of Eq. 33 is, in principle, an approximate version of Eq. 32 with a tolerance error of $O(\beta^4)$ and a trade-off of the mathematical complexity. For the sake of calculational convenience, α and β are interchangeably used in the rest of this article. By applying the boundary conditions of Eqs. 21–24, one finds

$$f_{\text{CPA}}(\eta) = \frac{1}{2} \left[\frac{2\sqrt{\eta}J_1(\alpha\sqrt{\eta}) - \alpha\eta J_0(\alpha)}{2J_1(\alpha) - \alpha J_0(\alpha)} \right] \quad (34)$$

where subscript ‘‘CPA’’ emphasizes the underlying assumption of the constant permeability (See Appendix C for details of coefficient determination.). Equation 34 converges to YF’s full solution based on the constant flux assumption as α reaches zero:

$$f_{\text{CFA}}(\eta) \rightarrow f_{\text{YF}}^0(\eta) = \eta - \frac{1}{2}\eta^2 + O(R_w) \quad (35)$$

(See Appendix D for details of a series expansion of the perturbation function f_{CPA}).

The dimensionless stream function for a small R_w is thus represented as

$$\Psi_{\text{CPA}} = f(\eta) \sinh \beta\xi = \frac{1}{2} \left[\frac{2\sqrt{\eta}J_1(\alpha\sqrt{\eta}) - \alpha\eta J_0(\alpha)}{2J_1(\alpha) - \alpha J_0(\alpha)} \right] \sinh \beta\xi \quad (36)$$

and the velocity components are derived as

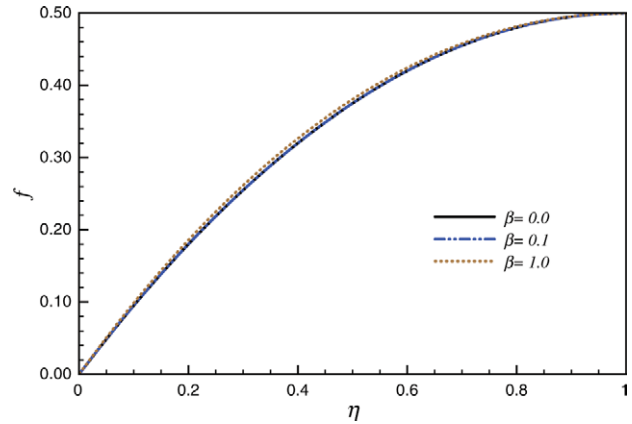


Figure 2. Plots of the perturbation function $f_{\text{CPA}}(\eta)$ of Eq. 34 vs. η for $\beta = 0, 0.1$ and 1.0 .

Lines for $\beta = 0.0$ and 0.1 are indistinguishable. The shape of $f_{\text{CPA}}(\eta)$ determines velocity components, u and v , of Eqs. 19 and 20, respectively. [Color figure can be viewed in the online issue, which is available at wileyonlinelibrary.com.]

$$u_{\text{CPA}} = 2\sqrt{2} \left[\frac{J_0(\alpha\sqrt{\eta}) - J_0(\alpha)}{2J_1(\alpha) - \alpha J_0(\alpha)} \right] \sinh \beta\xi \quad (37)$$

$$v_{\text{CPA}} = -\frac{1}{\sqrt{\eta}} \left[\frac{2\sqrt{\eta}J_1(\alpha\sqrt{\eta}) - \alpha\eta J_0(\alpha)}{2J_1(\alpha) - \alpha J_0(\alpha)} \right] \cosh \beta\xi \quad (38)$$

Finally, we approximated the pressure gradients of Eqs. 28 and 29 for a small R_w , substituted the perturbation function f_{CPA} of Eq. 34, and calculated the pressure distribution as

$$p_{\text{CPA}}(\eta, \xi) = -\Delta p_{m,0} \cosh \beta\xi \frac{J_0(\alpha\sqrt{\eta}) + J_0(\alpha)}{16\alpha^{-3}[2J_1(\alpha) - \alpha J_0(\alpha)]} \quad (39)$$

which is set to zero at the dead-end epi-center, where

$$\Delta p_{m,0} = \frac{\Delta P_{m,0}}{\rho V_{w0}^2} = \frac{vR_m}{V_{w0}} \quad (40)$$

Results and Discussion

Figure 2 shows that β does not significantly influence the perturbation function $f_{\text{CPA}}(\eta)$ when $0 \leq \beta \leq 1$. Note that the (positive) parameter β in principle of perturbation theory cannot exceed 1. Our solution for $f_{\text{CPA}}(\eta)$ with $\beta \rightarrow 0$ is equivalent to that of the constant flux approximation with $R_w \rightarrow 0$, denoted as $f_{\text{YF}}^0(\eta)$ in Eq. 35. As shown in Table 2, large membrane resistance generates very small values of β and R_w , having a relationship of $R_w = J_0 a / v = \Delta P \rho a^2 \beta^2 / 16\mu^2$. This makes constant flux and permeability approximations practically indistinguishable, especially for membranes of short lengths. The primary functional form of the perturbation function, $f_{\text{YF}}^0(\eta)$, seems to be universal to both constant flux and permeability approximations for small R_w s regardless of the membrane length. Nevertheless, it is worth investigating how much the small difference of dimensionless perturbation function f_{CPA} due to β can influence velocity components far away from the dead end. We approximated a difference

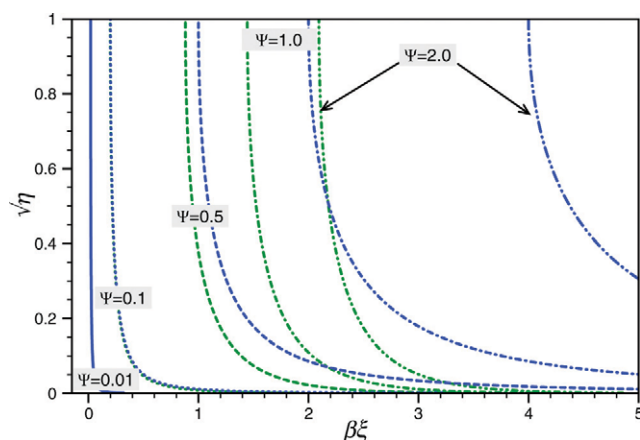


Figure 3. Streamlines from the CPA (green) and the CFA (blue) where Ψ_{CPA} is 0.01 (solid), 0.1 (dotted), 0.5 (dashed), 1.0 (dash-dotted), and 2.0 (long-dash-double-dotted).

For small Ψ_{CPA} values such as 0.01 and 0.1, streamlines of CPA and CFA are indistinguishable. All streamlines indicate fluid entering perpendicular to the membrane surface and flowing toward the open-end epi-center. [Color figure can be viewed in the online issue, which is available at wileyonlinelibrary.com.]

between $-v$ with a small but finite β and that of $\beta \rightarrow 0$ at the open-end surface (i.e., $\xi = l$ and $\eta = 1$):

$$-\Delta v = -v_{CPA} - (-v)_{CFA} \approx -\beta \frac{\partial v}{\partial \beta} = \beta l \sinh \beta l \quad (41)$$

and likewise

$$\Delta u = u_{CPA} - u_{CFA} \approx \beta \frac{\partial u}{\partial \beta} = 4l \frac{\beta l \cosh \beta l - \sinh \beta l}{\beta l} \quad (42)$$

at the open-end epi-center (i.e., $\xi = l$ and $\eta = 0$), where v_{CFA} and u_{CFA} indicate v_{CPA} and u_{CPA} at the limit of $\beta \rightarrow 0$. The hyperbolic terms of Eqs. 41 and 42 represent the exponential variation along the axial direction. Using the typical magnitude of $\beta l = O(1)$ for MF/UF, $-\Delta v$ can be much larger than βl and Δu is at least on the order of the dimensionless length, i.e., $O(l)$. This indicates that although effects of β on the shape of $f_{CPA}(\eta)$ are not easily noticeable in Figure 2, the small difference can drastically augment flow velocities at the open end. Even for the NF/RO group of $\beta l = O(10^{-1})$ or less, Δu are of an order of $l \times O(\beta^2 l^2)$, which also support that the crossflow velocity can significantly increase near the open end of a long HF membrane of a constant permeability.

Figure 3 presents streamlines calculated using the constant flux and permeability approximations. In general, the flow enters normal to the membrane surface due to the no-slip boundary condition and gradually approaches the epi-center in the orthogonal plane consisting of $\beta\xi$ and $\sqrt{\eta}$. The streamline for a small Ψ_{CPA} ($= 0.01$) indicates the fluid flow entering very near the dead end, which is consistently perpendicular to the membrane surface, even close to the epi-center. In this region, the radial velocity is (much) faster than the crossflow velocity because a permeate flux has not yet accumulated enough to generate the axial velocity of the

same order of magnitude as the permeate flux. A faster axial velocity is developed far from the dead end, at least a distance larger than the membrane half-radius as indicated in Eq. 27. A higher Ψ_{CPA} value implies a streamline entering farther from the dead end and approaching the channel epi-center much more gradually than those of small Ψ_{CPA} values. A noticeable deviation of stream functions between our constant permeability approximation and YF's constant flux approximation is clearly noticed in Figure 3. As Ψ_{CPA} increases, CFA-streamlines over-predict the entering point of fluid flow into the membrane interior, and in general provide more gradual variations in the streamlines. This discrepancy is negligible for short membranes of which maximum Ψ_{CPA} (corresponding to the membrane length) is small (i.e., $\Psi_{CPA} = O(10^{-2})$ or less), but is transparent for long membranes with $\beta l = O(1)$ or more.

Figure 4 compares flow profiles of u and v calculated using the constant flux and permeability approximations. The radial variations are solely governed by the perturbation function $f_{CPA}(\eta)$ so that the ratios, $R_U = u_{CPA}/u_{CFA}$ and $R_V = v_{CPA}/v_{CFA}$ vary along the axial distance only. If the membrane length is short, satisfying (at least) $\beta l < 1$, then the constant flux and permeability approximations show similar velocity profiles in magnitude as implied in Figure 3. The constant flux approximation, however, underestimates the permeate velocity as $\beta\xi$ exceeds 1, implying its failure near the open end of a long membrane channel. The crossflow velocity ratio R_U is always greater than the permeate velocity ratio R_V because the constant permeability approximation calculates the crossflow velocity by integrating the permeate flux from the dead end.

In this work, we studied basics of fluid mechanics in an HF membrane module and investigated effects of the dimensionless parameter, $\beta l (= 4L/\sqrt{R_m a^3})$ representing a characteristic membrane length, on the profiles of pressure distribution and velocity components. We here discuss implications of our results for real HF membrane processes. For NF/RO, HF membrane processes, one can readily use YF's constant

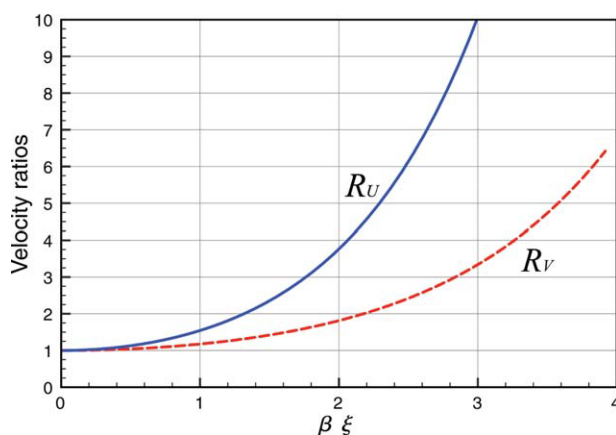


Figure 4. Comparison of constant permeability and flux approximations in terms of velocity ratios of $R_U = u_{CPA}/u_{CFA}$ (solid line) and $R_V = v_{CPA}/v_{CFA}$ (dotted-line).

Noticeable deviations of R_U and R_V from 1 indicate failure of the constant flux approximation. [Color figure can be viewed in the online issue, which is available at wileyonlinelibrary.com.]

flux approximation to estimate membrane performance in the presence of solute ions of feed water, presuming that the transmembrane pressure is also a quasi-constant along the membrane channel.⁵⁹ Even if the axial variation of solute concentration polarization is taken into account,^{60,61} standard film theory⁶² can provide a reasonable estimation of NF/RO membrane performance in terms of water recovery and solute rejection. This is because the solute concentration profiles have very gradual variation along the axial direction of membranes.⁶³ On the other hand, low hydraulic resistance of MF/UF membranes generates βl on the order of $O(1)$ or more as mentioned above and creates exponential profiles of the pressure and flow fields. The concept of critical flux has been argued for its constant character for long term operations.^{64,65} However, it is generally accepted that excessive transmembrane pressure accelerates solute accumulation on the membrane surface and does not effectively increase the permeate flux: filtration performance will be confined within the limiting flux regime.^{64,66} When the permeate flux at the open end is excessively high even though the length-averaged permeate flux is still in the region of the normal operation (i.e., below critical or sustaining flux), membrane fouling can occur near the open end and propagates to the dead end.^{11,54} This is opposite to the direction of the axial development of the concentration polarization in regular processes of spiral wound RO membranes. For constant flux operations, rapid solute accumulation can increase applied pressure, which may require frequent cleaning. Therefore, monitoring the permeate flux at the open end (where negative pressure is applied) can provide a practical indicator to prevent the initiation and propagation of (potential) membrane fouling. Furthermore, the stiffly changing, exponential profile of the permeate velocity can easily break the quasi-steady state in the presence of particulate foulant of feed water, and promote fouling.⁵⁴ To mitigate the onset of the fouling phenomena, this theory suggests the use of short HF membranes (especially for MF/UF processes) to keep the characteristic membrane length smaller than one, i.e., $\beta l < 1$.

Conclusions

We developed a perturbation theory for a laminar flow with injection to a cylindrical porous tube and applied it specifically to a hollow fiber membrane module of an arbitrary length and a small wall Reynolds number. Analytic expressions of the axial and radial velocities, and the pressure profile were derived by solving the Navier-Stokes and continuity equations. The conventional constant flux approximation was verified as a good approximation only for membranes of short lengths satisfying (at least) $\beta l < 1$ and large membrane resistances rendering $R_w \ll 1$. Long membranes having $\beta l > 1$, as used for MF and UF, have exponentially increasing pressure and velocity components in the axial direction,²¹ as proven by the constant permeability approximation used in this study. Discrepancies between constant flux and permeability approximations were observed in streamlines and velocity ratios especially far from the dead end of the long membrane ($\beta \xi > 1$). For membranes used for pressure-driven filtration, constant flux and permeability approximations have almost indistinguishable velocity variations in the radial direction due to the low values of the transport parameter β ; however, the small change of f due to finite β (or βl)

causes the noticeable velocity augmentation near the open end of a long membrane. In general, the constant permeability approximation unifies constant flux approximation and provides accurate fluid mechanics within HF membranes of arbitrary lengths. Specifically, a smaller value for βl of the NF/RO group than that of MF/UF makes the constant flux approximation reasonably accurate, generating the linear pressure profile in the axial direction. On the other hand, the MF/UF group requires the constant permeability approximation for a βl on the order of $O(1)$ or more, having fluid velocities and pressure distribution exponentially varying along the membrane channel in the flow direction. This drastic increase of the permeate flux may require careful setup of the negative pressure in terms of the membrane resistance and length to prevent fouling phenomena.

Acknowledgments

This research was supported by a grant from the US National Science Foundation Faculty Early Career (CAREER) Development Program (CBET04-49431) and the International Scholar Program of Kyung Hee University, Korea.

Literature Cited

- Zhongwei D, Liying L, Runyu M. Study on the effect of flow maldistribution on the performance of the hollow fiber modules used in membrane distillation. *J Membr Sci.* 2003;215:11–23.
- Busch J, Cruse A, Marquardt W. Modeling submerged hollow-fiber membrane filtration for wastewater treatment. *J Membr Sci.* 2007; 288:94–111.
- Severojr J, Almeida S, Narain N, Souza R, Santana J, Tambourg E. Wine clarification from *Spondias mombin* L. pulp by hollow fiber membrane system. *Process Biochem.* 2007;42:1516–1520.
- Tasselli F, Cassano A, Drioli E. Ultrafiltration of kiwifruit juice using modified poly(ether ether ketone) hollow fibre membranes. *Sep Purif Technol.* 2007;57:94–102.
- Basu R, Sirkar KK. Pharmaceutical product recovery using a hollow fiber contained liquid membrane: a case study. *J Membr Sci.* 1992; 75:131–149.
- Lazarova Z, Syska B, Schügerl K. Application of large-scale hollow fiber membrane contactors for simultaneous extractive removal and stripping of penicillin G. *J Membr Sci.* 2002;202:151–164.
- Larsson N, Utterback K, Toräng L, Risberg J, Gustafsson P, Mayer P, Jönsson JÅ. Equilibrium sampling through membranes (ESTM) of acidic organic pollutants using hollow fibre modules in continuous steady-state mode. *Chemosphere.* 2009;76:1213–1220.
- Pankhania M, Stephenson T, Semmens MJ. Hollow fibre bioreactor for wastewater treatment using bubbleless membrane aeration. *Water Res.* 1994;28:2233–2236.
- Yang Q, Kocherginsky N. Copper removal from ammoniacal wastewater through a hollow fiber supported liquid membrane system: modeling and experimental verification. *J Membr Sci.* 2007;297:121–129.
- Alberti F, Bienati B, Bottino A, Capannelli G, Comite A, Ferrari F, Firpo R. Hydrocarbon removal from industrial wastewater by hollow-fiber membrane bioreactors. *Desalination.* 2007;204:24–32.
- Yoon SH, Lee S, Yeom IT. Experimental verification of pressure drop models in hollow fiber membrane. *J Membr Sci.* 2008;310:7–12.
- Yoon SH, Kim HS, Yeom IT. Optimization model of submerged hollow fiber membrane modules. *J Membr Sci.* 2004;234:147–156.
- Cath T, Childress A, Elimelech M. Forward osmosis: principles, applications, and recent developments. *J Membr Sci.* 2006;281:70–87.
- Tang W, Ng H. Concentration of brine by forward osmosis: performance and influence of membrane structure. *Desalination.* 2008; 224:143–153.
- Wang K, Chung TS, Qin JJ. Polybenzimidazole (PBI) nanofiltration hollow fiber membranes applied in forward osmosis process. *J Membr Sci.* 2007;300:6–12.
- Su J, Yang Q, Teo J, Chung TS. Cellulose acetate nanofiltration hollow fiber membranes for forward osmosis processes. *J Membr Sci.* 2010;355:36–44.

17. Wang R, Shi L, Tang C, Chou S, Qiu C, Fane A. Characterization of novel forward osmosis hollow fiber membranes. *J Membr Sci.* 2010;355:158–167.
18. Xu X, Li J, Li H, Cai Y, Cao Y, He B, Zhang Y. Non-invasive monitoring of fouling in hollow fiber membrane via UTDR. *J Membr Sci.* 2009;326:103–110.
19. Carroll T, Booker NA. Axial features in the fouling of hollow-fibre membranes. *J Membr Sci.* 2000;168:203–212.
20. Chang S, Yeo A, Fane A, Cholewa M, Ping Y, Moser H. Observation of flow characteristics in a hollow fiber lumen using non-invasive X-ray microimaging (XMI). *J Membr Sci.* 2007;304:181–189.
21. Chang S, Fane A, Waite T. Analysis of constant permeate flow filtration using dead-end hollow fiber membranes. *J Membr Sci.* 2006;268:132–141.
22. Hong S, Bae T, Tak T, Hong S, Randall A. Fouling control in activated sludge submerged hollow fiber membrane bioreactors. *Desalination.* 2002;143:219–228.
23. Berman AS. Laminar flow in channels with porous walls. *J Appl Phys.* 1953;24:1232–1235.
24. Yuan SW, Finkelstein AB. Laminar pipe flow with injection and suction through a porous wall. *Trans ASME.* 1956;78:719–724.
25. Berman AS. Concerning laminar flow in channels with porous walls. *J Appl Phys.* 1956;27:1557–1558.
26. Terrill R, Thomas P. On laminar flow through a uniformly porous pipe. *Appl Sci Res.* 1969;21:37–67.
27. Chellam S, Liu M. Effect of slip on existence, uniqueness, and behavior of similarity solutions for steady incompressible laminar flow in porous tubes and channels. *Phys Fluids.* 2006;18:083601.
28. Brady JF, Acrivos A. Steady flow in a channel or tube with an accelerating surface velocity. an exact solution to the Navier-Stokes equations with reverse flow. *J Fluid Mech.* 1981;112:127–150.
29. Belfort G, Davis RH, Zydney AL. The behavior of suspensions and macromolecular solutions in crossflow microfiltration. *J Membr Sci.* 1994;96:1–58.
30. Bouchard C, Carreau P, Matsuura T, Sourirajan S. Modeling of ultrafiltration: predictions of concentration polarization effects. *J Membr Sci.* 1994;97:215–229.
31. Denisov GA. Theory of concentration polarization in cross-flow ultrafiltration: gel-layer model and osmotic-pressure model. *J Membr Sci.* 1994;91:173–187.
32. Lee Y, Clark M. Modeling of flux decline during crossflow ultrafiltration of colloidal suspensions. *J Membr Sci.* 1998;149:181–202.
33. Belfort G. Membrane modules: comparison of different configurations using fluid mechanics. *J Membr Sci.* 1988;35:245–270.
34. Wiley D, Fletcher D. Techniques for computational fluid dynamics modelling of flow in membrane channels. *J Membr Sci.* 2003;211:127–137.
35. Ghidossi R, Daurrelle J, Veyret D, Moulin P. Simplified CFD approach of a hollow fiber ultrafiltration system. *Chem Eng J.* 2006;123:117–125.
36. Potts DE, Ahlert RC, Wang SS. A critical review of fouling of reverse osmosis membranes. *Desalination.* 1981;36:235–264.
37. Williams F. Linearized analysis of constant-property duct flows. *J Fluid Mech.* 1968;34:241–261.
38. Mishra S, Roy J. Laminar elasticoviscous flow in an annulus with porous walls. *Phys Fluids.* 1967;10:2300–2304.
39. Skalak F, Wang CY. Pulsatile flow in a tube with wall injection and suction. *Appl Sci Res.* 1977;33:269–307.
40. Thorman J, Hwang ST. Compressible flow in permeable capillaries under deformation. *Chem Eng Sci.* 1978;33:15–20.
41. Majdalani J, Flandro GA. The oscillatory pipe flow with arbitrary wall injection. *Proc R Soc A.* 2002;458:1621–1651.
42. Kinney R. Fully developed frictional and heat-transfer characteristics of laminar flow in porous tubes. *Int J Heat Mass Transf.* 1968;11:1393–1401.
43. Raithby G. Laminar heat transfer in the thermal entrance region of circular tubes and two-dimensional rectangular ducts with wall suction and injection. *Int J Heat Mass Transf.* 1971;14(2):223–243.
44. Wang P, Wehrmeyer J, Pitz R. Stretch rate of tubular premixed flames. *Combust Flame.* 2006;145:401–414.
45. Lim S, Tan X, Li K. Gas/vapour separation using membranes: effect of pressure drop in lumen of hollow fibres. *Chem Eng Sci.* 2000;55:2641–2652.
46. Monge LE. Improved reverse osmosis permeation by heating. *J Food Sci.* 2006;38:633–636.
47. Deng X, Marois Y, How T, Merhi Y, King M, Guidoin R. Luminal surface concentration of lipoprotein (LDL) and its effect on the wall uptake of cholesterol by canine carotid arteries. *J Vasc Surg.* 1995;21:135–145.
48. Friedlander S, Walser M. Some aspects of flow and diffusion in the proximal tubule of the kidney. *J Theor Biol.* 1965;8:87–96.
49. Jacquez J, Foster D, Daniels E. Solute concentration in the kidney. I. A model of the renal medulla and its limit cases. *Math Biosci.* 1976;32:307–335.
50. Moussy Y. Bioartificial kidney. I. Theoretical analysis of convective flow in hollow fiber modules: application to a bioartificial hemofilter. *Biotech Bioeng.* 2000;68:142–152.
51. Reay D, Thiele F. Heat pipe theory applied to a biological system: quantification of the role of the “resting” eccrine sweat gland in thermoregulation. *J Theor Biol.* 1977;64:789–803.
52. Karode S. Laminar flow in channels with porous walls, revisited. *J Membr Sci.* 2001;191:237–241.
53. Kozinski AA, Schmidt FP, Lightfoot EN. Velocity profiles in porous-walled ducts. *Ind Eng Chem Fundam.* 1970;9:502–505.
54. Kim J, DiGiano F. Defining critical flux in submerged membranes: influence of length-distributed flux. *J Membr Sci.* 2006;280:752–761.
55. The American Water Works Research Foundation. *Water Treatment Membrane Processes.* New York: McGraw-Hill, 1996.
56. Zeman LJ, Zydney AL. *Microfiltration and Ultrafiltration: Principles and Applications.* New York: Marcel Dekker, Inc. 1996.
57. Richard WBaker L. *Membrane Technology and Applications*, 2nd ed. West Sussex, England: Wiley, 2004.
58. Mulder M. *Basic Principles of Membrane Technology.* Boston, MA: Kluwer Academic Publications, 1996.
59. Zydney A. Stagnant film model for concentration polarization in membrane systems. *J Membr Sci.* 1997;130:275–281.
60. Bhattacharyya D, Back S, Kermod R, Roco M. Prediction of concentration polarization and flux behavior in reverse osmosis by numerical analysis. *J Membr Sci.* 1990;48:231–262.
61. Kim AS. Permeate flux inflection due to concentration polarization in crossflow membrane filtration: a novel analytic approach. *Eur Phys J E.* 2007;24:331–341.
62. Michaels AS. New separation technique for the CPI. *Chem Eng Prog.* 1968;64:31–43.
63. Bacchin P. A possible link between critical and limiting flux for colloidal systems: consideration of critical deposit formation along a membrane. *J Membr Sci.* 2004;228:237–241.
64. Bacchin P, Aimar P, Field RW. Critical and sustainable fluxes: theory, experiments and applications. *J Membr Sci.* 2006;281:42–69.
65. Kim AS, Liu Y. Critical flux of hard sphere suspensions in cross-flow filtration: hydrodynamic force bias Monte Carlo simulations. *J Membr Sci.* 2008;323:67–76.
66. Song L. A new model for the calculation of the limiting flux in ultrafiltration. *J Membr Sci.* 1998;144:173–185.

Appendix A: Mathematical Identities

The original Navier-Stokes and continuity equations in the cylindrical coordinates are as follows:

$$-\frac{\partial P}{\partial z} = \rho \left(V \frac{\partial U}{\partial r} + U \frac{\partial U}{\partial z} \right) - \mu \left(\frac{1}{r} \frac{\partial}{\partial r} \left(r \frac{\partial U}{\partial r} \right) + \frac{\partial^2 U}{\partial z^2} \right) \quad (\text{A1})$$

$$-\frac{\partial P}{\partial r} = \rho \left(V \frac{\partial V}{\partial r} + U \frac{\partial V}{\partial z} \right) - \mu \left(\frac{\partial}{\partial r} \left(\frac{1}{r} \frac{\partial (rV)}{\partial r} \right) + \frac{\partial^2 V}{\partial z^2} \right) \quad (\text{A2})$$

and

$$\frac{1}{r} \frac{\partial (rV)}{\partial r} + \frac{\partial U}{\partial z} = 0 \quad (\text{A3})$$

where the transient and azimuthal terms are not included due to assumptions used in Eqs. 3–5. Transformation of differential operators from (r, z) to (η, ζ) coordinates are used:

$$\frac{\partial}{\partial r} = \frac{2}{a} \sqrt{\eta} \frac{\partial}{\partial \eta} \quad (\text{A4a})$$

$$r \frac{\partial}{\partial r} = 2\eta \frac{\partial}{\partial \eta} \quad (\text{A4b})$$

$$\frac{1}{r} \frac{\partial}{\partial r} = \frac{2}{a^2} \frac{\partial}{\partial \eta} \quad (\text{A4c})$$

$$\frac{1}{r} \frac{\partial}{\partial r} \left(r \frac{\partial}{\partial r} \right) = \frac{4}{a^2} \frac{\partial}{\partial \eta} \left(\eta \frac{\partial}{\partial \eta} \right) \quad (\text{A5d})$$

and

$$\frac{\partial}{\partial z} = \frac{1}{a} \frac{\partial}{\partial \xi} \quad (\text{A5a})$$

$$\frac{\partial^2}{\partial z^2} = \frac{1}{a^2} \frac{\partial^2}{\partial \xi^2} \quad (\text{A5b})$$

Appendix B: Wall Velocity Variation Along the z-Direction

In this section, we derive an asymptotic representation of the wall velocity V_w when the length of the HF membrane is much longer than the tube radius to emphasize the axial variation only. Using Darcy's law, the permeate velocity (in magnitude), defined as $V_w = -V$ ($r = a, z$), is assumed to be proportional to the transmembrane pressure:

$$V_w(z) = \frac{P_{\text{out}} - P_w(z)}{\mu R_m} \quad (\text{B1})$$

where P_{out} and $P_w(z)$ are the pressures on the exterior and interior surfaces, respectively, of the HF module at a distance z from the dead end. Because one end of the membrane is blocked, the crossflow rate Q measured at z is calculated as the accumulation of the permeate flux along the membrane channel:

$$Q(z) = 2\pi a \int_0^z V_w(z') dz' \quad (\text{B2})$$

By modifying the original Hagen-Poiseuille equation, the axial gradient of the flow rate can be approximated⁵² as

$$\frac{\partial Q}{\partial z} = 2\pi a V_w(z) = \frac{\pi a^4}{8\mu} \left(-\frac{\partial^2 P}{\partial z^2} \right) \quad (\text{B3})$$

assuming that the internal crossflow is fully developed for $z > 0$, and the radial dependency of the pressure is negligible.

Substitution of Eq. B1 into Eq. B3 gives a second-order ordinary differential equation:

$$\frac{d^2 P_w^*}{dz^2} - \lambda^2 P_w^* = 0 \quad (\text{B4})$$

where

$$P_w^*(z) = P_w(z) - P_{\text{out}} \quad (\text{B5})$$

$$\lambda = \frac{4}{\sqrt{R_m a^3}} \quad (\text{B6})$$

An infinite membrane resistance (i.e., $\lambda \rightarrow 0$) mimics the impermeable rigid pipe with the linear pressure distribution.⁵⁴ The boundary conditions for Eq. B4 are

$$P_w^*(z=0) = -\Delta P_{m,0} \quad (\text{B7})$$

$$\left. -\frac{dP_w^*}{dz} \right|_{z=0} = 0 \quad (\text{B8})$$

where $\Delta P_{m,0}$ indicates the transmembrane pressure (in magnitude) on the porous wall at the dead end. The solution for P_w is

$$P_w(z) = P_{\text{out}} - \Delta P_{m,0} \cosh \lambda z \quad (\text{B9})$$

and the pressure drop along the entire membrane channel is calculated as

$$|\Delta P_L| = P_0 - P_L = -\Delta P_L \quad (\text{B10})$$

where $P_0 = P_w(z=0)$ and $P_L = P_w(z=L)$ as shown in Fig. 1. Note that Eq. B9 originates from applying the mass balance approximation of Eq. B3 based on the Hagen-Poiseuille equation—not directly from solving the Navier-Stokes equation.

Using Eq. B9, the wall flux V_w is then represented as

$$V_w(z) = V_{w0} \cosh \lambda z \quad (\text{B11})$$

where

$$V_{w0} = \frac{\lambda^2 a^3}{16\mu} \Delta P_{m,0} = \frac{\Delta P_{m,0}}{\mu R_m} \quad (\text{B12})$$

Appendix C: Determination of C_1 – C_4

Unknown coefficients, C_1 – C_4 , of Eq. 33 are determined as follows:

(i) Applying BC Eqs. 23–33 yields

$$\lim_{\eta \rightarrow 0} \frac{f(\eta)}{\sqrt{\eta}} \rightarrow \frac{C_1}{\sqrt{\eta}} + C_4 Y_1(\alpha \sqrt{\eta}) \approx \frac{1}{\sqrt{\eta}} \left[C_1 - \frac{2}{\alpha \pi} C_4 \right] = 0 \quad (\text{C1})$$

so that

$$C_1 = \frac{2}{\alpha \pi} C_4 \quad (\text{C2})$$

using

$$Y_1(x) = -\frac{2}{\pi x} + \left(\frac{-\ln(2) + \ln(x)}{\pi} - 1/2 \frac{-2\gamma + 1}{\pi} \right) x + \dots \quad (\text{C3})$$

(ii) From BC Eq. 24

$$\lim_{\eta \rightarrow 0} \sqrt{\eta} f''(\eta) \rightarrow C_3 \sqrt{\eta} \frac{d^2}{d\eta^2} [\sqrt{\eta} J_1(\alpha\sqrt{\eta})] + C_4 \sqrt{\eta} \frac{d^2}{d\eta^2} [\sqrt{\eta} Y_1(\alpha\sqrt{\eta})] = 0 \quad (\text{C4})$$

Because

$$J_1(x) = \frac{1}{2}x - \frac{1}{16}x^3 + \dots \quad (\text{C5})$$

the first term of Eq. C4 vanishes as $\eta \rightarrow 0$. The x^{-1} term of Eq. C2 causes the divergence of the second term of Eq. C4 as η reaches zero so that $C_4 = 0$ should be satisfied, and therefore $C_1 = 0$.

(iii) BC Eqs. 21 and 22 easily determine the rest of unknown constants, C_2 and C_3 , to provide the final solution of Eq. 34.

Appendix D: Series Expansion of $f(\eta)$ for a Small R_w

The series expansion of Eq. 34 yields

$$f(\eta) = \frac{2\sqrt{\eta}J_1(\alpha\sqrt{\eta}) - \alpha\eta J_0(\alpha)}{2[2J_1(\alpha) - \alpha J_0(\alpha)]} = \frac{\alpha^3 F(\eta)}{\alpha^3 G(\alpha)} = \frac{F(\eta)}{G(\alpha)} \quad (\text{D1})$$

where

$$F(\eta) = \sum_{m=0}^{\infty} \left(\eta - \frac{1}{m+2} \eta^{m+2} \right) \frac{\alpha^{2m}}{F_m} \quad (\text{D2})$$

$$G(\alpha) = \sum_{m=0}^{\infty} \frac{1}{G_m} \alpha^{2m} \quad (\text{D3})$$

Using Eq. C5 and

$$J_0(x) = 1 - \frac{1}{4}x^2 + \frac{1}{64}x^4 + \dots \quad (\text{D4})$$

we here derived recurrence formulae for F_m and G_m as

$$F_m = (-1)^m 4(m+1)^2 F_{m-1}, \quad F_0 = 1 \quad (\text{D5})$$

$$G_m = (-1)^m 2m(2m+4) G_{m-1}, \quad G_0 = 1 \quad (\text{D6})$$

respectively, and we have

$$F(\eta) = \left(\eta - \frac{\eta^2}{2} \right) - \frac{\alpha^2}{64} \left(\eta - \frac{\eta^3}{3} \right) + \frac{\alpha^4}{576} \left(\eta - \frac{\eta^4}{4} \right) - \frac{\alpha^6}{36864} \left(\eta - \frac{\eta^5}{5} \right) + \dots \quad (\text{D7})$$

and

$$G(\alpha) = 1 - \frac{\alpha^2}{12} + \frac{\alpha^4}{384} - \frac{\alpha^6}{23040} + \dots \quad (\text{D8})$$

Manuscript received May 28, 2010, and revision received Aug. 31, 2010.